A Long-Term Record of Aerosol Optical Depth from TOMS Observations and Comparison to AERONET Measurements

O. TORRES

Joint Center for Earth Systems Technology, University of Maryland Baltimore County, Baltimore, Maryland

P. K. BHARTIA AND J. R. HERMAN

Laboratory for Atmospheres, NASA Goddard Space Flight Center, Greenbelt, Maryland

A. SINYUK

Joint Center for Earth Systems Technology, University of Maryland Baltimore County, Baltimore, Maryland

PAUL GINOUX

Georgia Institute of Technology, Atlanta, Georgia

BRENT HOLBEN

Laboratory for Atmospheres, NASA Goddard Space Flight Center, Greenbelt, Maryland

(Manuscript received 8 January 2001, in final form 17 July 2001)

ABSTRACT

Observations of backscattered near-ultraviolet radiation from the Total Ozone Mapping Spectrometer (TOMS) on board the *Nimbus-7* (1979–92) and the *Earth Probe* (mid-1996 to present) satellites have been used to derive a long-term record of aerosol optical depth over oceans and continents. The retrieval technique applied to the TOMS data makes use of two unique advantages of near-UV remote sensing not available in the visible or near-IR: 1) low reflectivity of all land surface types (including the normally bright deserts in the visible), which makes possible aerosol retrieval over the continents; and 2) large sensitivity to aerosol types that absorb in the UV, allowing the clear separation of carbonaceous and mineral aerosols from purely scattering particles such as sulfate and sea salt aerosols. The near-UV method of aerosol characterization is validated by comparison with Aerosol Robotic Network (AERONET) ground-based observations. TOMS retrievals of aerosol optical depth over land areas (1996–2000) are shown to agree reasonably well with AERONET sun photometer observations for a variety of environments characterized by different aerosol types, such as carbonaceous aerosols from biomass burning, desert dust aerosols, and sulfate aerosols. In most cases the TOMS-derived optical depths of UV-absorbing aerosols are within 30% of the AERONET observations, while nonabsorbing optical depths agree to within 20%. The results presented here constitute the first long-term nearly global climatology of aerosol optical depth over both land and water surfaces, extending the observations of aerosol optical depth to regions and times (1979 to present) not accessible to ground-based observations.

1. Introduction

Tropospheric aerosols influence the earth's climate in many ways, not all of them well known. The direct cooling effect of aerosols on climate, by scattering a fraction of the incoming solar radiation back to space, is well understood. The radiative heating effects produced by aerosol absorption of short- and longwave radiation has been found to produce changes in net heating rates (Alpert et al. 1998). Aerosol heating effects can in turn produce changes in atmospheric circulation (Miller and Tegen 1998). In addition, aerosols can indirectly affect climate through their action as cloud condensation nuclei. The evaluation of aerosol radiative forcing effect on climate (the net radiation flux change at the top of the atmosphere due solely to the effect of atmospheric aerosols), requires global data on aerosol properties and amounts over both the oceans and the continents. Since any potential for global climate change is closely associated with the effect of man's activities, the availability of long-term aerosol data sets is of critical importance to separate the aerosol effects of an-

Corresponding author address: Dr. O. Torres, NASA Goddard Space Flight Center, Code 916, Greenbelt, MD 20771.
E-mail: torres@tparty.gsfc.nasa.gov

thropogenic origin, from those generated by natural processes.

Aerosol effects are also significant in non-climate-related processes, such as those related to the analysis of local, regional, and global air pollution. Large-scale biomass burning and boreal forest fire events often cast huge smoke plumes thousands of kilometers away from their sources, causing serious air quality and health-related problems.

Increased levels of surface UV-B (290–315 nm) radiation levels, following stratospheric ozone layer depletion, have been reported at mid- and high latitudes. Since aerosols play a fundamental role in the attenuation of UV-B and UV-A (315–400 nm) radiation at the earth's surface, their radiative transfer effects must be carefully taken into account in assessments and modeling studies to quantify the effects on surface radiation from global ozone decreases and changes in both aerosol and cloud amounts.

The importance of aerosols in tropospheric chemistry is currently receiving a great deal of attention. It has been suggested that desert dust aerosols may contribute to decreases in tropospheric ozone by providing surfaces for heterogeneous chemistry processes that consume ozone (Dentener et al. 1996). Additional ozone reductions or enhancements may occur in the vicinity of the tropospheric aerosol layers, where the presence of aerosol scattering and absorption affect ozone (and other trace gas) photolysis rates. As discussed by Dickerson et al. (1997), observations and numerical models show that aerosol scattering of UV radiation in the boundary layer accelerate photochemical reactions and smog production, while UV-absorbing aerosols inhibit smog production. Finally, since aerosols also affect remote sensing of other geophysical parameters (e.g., ocean color, atmospheric ozone, surface albedo, etc.), accurate knowledge of aerosol properties is required for the application of atmospheric corrections to remove the aerosol effects.

Use of satellite observations is the most efficient way to determine aerosol physical properties on the temporal and spatial scales needed to understand and monitor their effects on the earth–atmosphere system. Traditional aerosol satellite-based retrievals have been limited to ocean areas that are dark in the visible and near IR (Stowe et al. 1997; Mishchenko et al. 1999). For land areas, the surface contribution to the reflected visible and near-IR is significantly larger than contributed by aerosols. Therefore, aerosol characterization over land with visible and near-IR observations is very difficult without a precise characterization of the surface radiative properties. In the near future, satellite-based aerosol sensing over land is expected to dramatically improve as instrumentation specifically designed for aerosol remote sensing begins the implementation of sophisticated algorithms making use of measurements at multiple wavelengths [moderate resolution imaging spectroradiometer (MODIS)] and viewing geometries [multiangle imaging spectroradiometer (MISR)]. In the last few years, an additional remote sensing tool for aerosol detection and characterization has been developed (Herman et al. 1997; Torres et al. 1998). The approach uses space-measured radiances in the 330–380-nm range by the Total Ozone Mapping Spectrometer (TOMS) family of instruments to retrieve optical depth and single scattering albedo of tropospheric aerosols over both land and water surfaces.

In this paper we present results of the application of the near-UV technique to retrieve aerosol properties using satellite-based measurements from the TOMS sensors. A brief discussion of the technique's physical basis is presented, followed by a description of the retrieval algorithm to derive optical depth and single scattering albedo. The performance of the near-UV method over land is evaluated by comparing the satellite derived optical depth to Aerosol Robotic Network (AERONET) ground-based observations. A detailed discussion on the single scattering albedo product and comparison with independent measurements will be published separately. The obtained global long-term record of aerosol optical depth is briefly discussed and a regional climatological analysis over selected areas of the world is carried out.

2. Aerosol characterization in the near-ultraviolet

a. Historic background

An approach to retrieve aerosol properties using measurements in the near-ultraviolet spectral region has emerged in the last few years (Torres et al. 1998). The aerosol detection capability in the near UV first became apparent with the development of the TOMS aerosol index (AI), as a by-product of the TOMS version 7 ozone algorithm (McPeters et al. 1996). The TOMS AI (Herman et al. 1997) is a surprisingly efficient method of space-based aerosol detection. The AI is a measure of the change of spectral contrast in the near ultraviolet due to radiative transfer effects of aerosols in a Rayleigh scattering atmosphere. By definition, AI is positive for absorbing aerosols, near zero (± 0.2) in the presence of clouds or large size (0.2 μm or larger) nonabsorbing aerosols and negative for small size nonabsorbing particles. The AI detects aerosols over all land and ocean surfaces, even those covered by ice/snow and over clouds (Hsu et al. 1999).

The AI has been used in a variety of applications, including mapping the global distribution of UV-absorbing aerosols (Herman et al. 1997), correcting for aerosol induced errors in the retrieval of column ozone amounts (Torres and Bhartia 1999), aerosol characterization from space during Smoke, Clouds, and Radiation-Brazil (SCAR-B; Gleason et al. 1998), identifying dust aerosol induced biases in retrieved sea surface temperature from brightness temperature measurements (Diaz et al. 2001), estimating UV reduction at the earth's surface (Herman et al. 1999; Krotkov et al. 1998), es-

timating the radiative forcing effects of mineral aerosols used in conjunction with Earth Radiation Budget Experiment (ERBE) data (Hsu et al. 2000), in the environmental characterization of soil dust sources (Prospero et al. 2002) and in the study of the interannual variability of soil dust aerosols in conjunction with Advanced Very High Resolution Radiometer (AVHRR) data (Cakmur et al. 2001). Although the AI is a very useful qualitative indicator of aerosol presence, an actual inversion procedure is required to interpret the measured radiance departures from a Rayleigh atmosphere model, in terms of traditional aerosol parameters such as optical depth, τ, and single scattering albedo, ω_0 (Torres et al. 1998).

b. Physical basis of the near-UV inversion method

To illustrate the physical basis of this approach to aerosol sensing, it is useful to consider a variation of the single scattering approximation, in which molecular multiple scattering effects are taken into account and only particle multiple scattering effects, as well as other second-order terms (reflected and then scattered radiation and vice versa), are neglected. Using this simplification, the radiance (I) at the top of an aerosol-laden atmosphere, as measured from a satellite instrument, is approximately given by the expression

$$I \approx \frac{\omega_0 P(\Theta)\pi F_0}{4\pi}[1 - e^{-\tau(1/\mu+1/\mu_0)}] + \left[\frac{p_s - p_a}{p_s}\right] \times [I_s + I_0]e^{-(1-\omega_0)\tau(1/\mu+1/\mu_0)} + \frac{p_a}{p_s}[I_s + I_0], \quad (1)$$

where ω_0 is aerosol single scattering albedo; Θ is scattering angle; $P(\Theta)$ is aerosol scattering phase function; τ is aerosol extinction optical depth; πF_0 is incoming solar flux; μ and μ_0 are, respectively, the cosines of the satellite and solar zenith angles; and p_s and p_a are surface and aerosol layer pressure levels, respectively. The term I_s represents the upward radiance reflected by the surface and transmitted through the atmosphere to the satellite, and I_0 is the Rayleigh scattered radiance. The first term on the right side of Eq. (1) is the singly scattered radiance added by the aerosol layer. The second term represents the fraction of Rayleigh scattered and surface reflected radiance below the aerosol layer. The third term is the fraction of Rayleigh scattered and surface reflected radiance reaching the atmospheric column above the aerosol layer, which is not affected by particle absorption effects. For a nonabsorbing aerosol layer (i.e., $\omega_0 = 1$), the aerosol effect in the second term vanishes, and the net aerosol effect is just the single scattering contribution.

A quick inspection of the above equation clearly shows the differences between the near-UV and visible-near-IR methods of space-based aerosol sensing and the source of sensitivity to aerosol absorption effects in the near UV. In the visible and near IR spectral regions, the term I_0 (mostly singly scattered radiation) is generally very small. The term I_s is also very small over water surfaces. Over most land surfaces, on the other hand, I_s is significantly larger than the contribution of aerosol scattering to the total radiance. Therefore, the detection of the aerosol effect is very difficult without a precise characterization of the surface albedo. For this reason, visible and IR satellite retrieval of aerosol properties from radiance measurements is generally limited to dark water surfaces where the aerosol information is mainly contained in the first term of Eq. (1).

In the near UV the quantity I_0 is much larger than its counterpart in the visible and cannot be neglected. Because of the interaction of aerosol absorption and multiple molecular scattering, Rayleigh scattering increases the length of a photon's path through an absorbing aerosol layer, so that the chance of aerosol absorption is significantly enhanced (Gordon et al. 1997). Since molecular scattering depends strongly on pressure, the magnitude of the second term of Eq. (1) is also a function of the height of the aerosol layer (i.e., p_a). The higher the layer of absorbing particles above the surface, the larger the fraction of molecular scattered radiation subject to absorption by aerosols. The effect of nonabsorbing aerosols does not depend on aerosol layer height, since their main role is to add singly scattered radiance to the preexisting scattered radiances from the atmosphere. The near-UV I_s term is generally low over both water and land surfaces (Herman and Celarier 1997). The ocean reflectivity is seldom larger than about 8%, whereas all vegetated surfaces show a reflectivity no larger than about 4%. The largest reflectivity of ice/snow free surfaces in the near UV corresponds to deserts with a typical value of about 8%. Thus, the low surface contribution to the total radiance at the top of the atmosphere in the near UV allows the retrieval of aerosol information over both water and land surfaces.

In summary, the sensitivity to aerosol absorption in the near UV derives from the large molecular scattering contribution characteristic of this spectral region. The capability of aerosol detection over the oceans and the continents comes from the low value of the near-UV albedo of most terrestrial surfaces.

c. Advantages and shortcomings of the near-UV approach

1) ADVANTAGES

The main advantages of the near-UV approach are the high sensitivity to particle absorption, and the capability of retrieving aerosol properties over most terrestrial surfaces including deserts. The low near-UV surface albedo results in reduced sensitivities to errors in assumed values of surface albedo as well as those associated with neglecting BRDF (bidirectional reflectivity distribution function) effects.

Another advantage of using near-UV measurements for aerosol sensing is the smaller sensitivity (than in visible and near-IR) to aerosol phase function effects. Since in the near-UV, multiple molecular scattering is a large component of the measured upwelling radiance at the top of the atmosphere, the effect of aerosol scattering phase function (a single scattering property) smears out, resulting in smaller (than in the visible) errors in retrieved aerosol properties when spherically shaped particles are assumed. Furthermore, the effect of particle shape on scattering properties of nonspherical aerosols becomes weaker with increasing imaginary component (absorption) of aerosol particle refractive indices (van de Hulst 1957). Since the imaginary refractive index of mineral dust in the UV wavelengths is significantly larger than in the visible–near-IR wavelengths (Patterson et al. 1977), the effect of nonspherical particle shape is less important (than at longer wavelengths) in the near-UV retrieval of mineral dust optical depth.

2) SHORTCOMINGS

Since the near-UV method of absorbing aerosol retrieval is based on the absorption by particles in the presence of molecular scattering, the retrieved quantities are sensitive to the height above the ground of the absorbing aerosol layer. The sensitivity to aerosol plume height is largest for strongly UV-absorbing aerosols and decreases rapidly with decreasing absorption (Torres et al. 1998). For nonabsorbing aerosols, the dependence on aerosol layer height is negligible.

Another difficulty of this technique is the decrease in sensitivity when a shallow ''gray'' (i.e., spectrally independent imaginary refractive index, such as smoke) absorbing aerosol layer of small optical depth (less than about 0.5) is confined to the bottom 1 km of the atmosphere, where the spectral signal of the aerosol absorption effect is significantly reduced. For ''colored'' aerosols (like mineral dust), the spectral dependence of the optical properties of the aerosol particles allows detection even when the aerosol layer is close to the ground.

The near-UV technique does an excellent job separating UV-absorbing from nonabsorbing aerosols. It cannot, however, distinguish between UV-absorbing aerosol types (i.e., carbonaceous and mineral dust aerosols), because the TOMS aerosol channels in the 330–380-nm range are not sufficiently separated to allow enough spectral contrast between these two aerosol types. Although, in most cases these aerosol types are geographically separated, there are regions such as the tropical Atlantic Ocean during the winter and early spring seasons, where either or both aerosol types may be present. The wrong choice of aerosol type will produce large errors in optical depth. For instance, the optical depth of mineral aerosols may be overestimated by as much as a factor of 2 if the carbonaceous aerosol model is mistakenly selected. By the same token, the erroneous choice of mineral dust models to retrieve carbonaceous aerosols yields an underestimate in optical depth.

Subpixel cloud contamination is a major source of uncertainty in the application of the near-UV algorithm to the TOMS data that results in overestimations of both optical depth and single scattering albedo (Torres et al. 1998). Since the TOMS family of sensors was not designed to measure aerosols, their field of view (FOV; of 40×40 km^2 at nadir and as large as 200×200 km^2 at extreme off-nadir viewing geometry) is clearly not optimized for aerosol sensing. Therefore the likelihood of intervening subpixel clouds in the instrument's FOV is very large.

3. TOMS aerosol algorithm

In the near-UV method, measurements of the backscattered radiance (I_λ) at two wavelengths λ_1 and λ_2, ($\lambda_2 > \lambda_1$) are used. Aerosol particles are characterized by examining the variability of the relationship between the spectral contrast ($I_{\lambda 1}/I_{\lambda 2}$) and the radiance at the longer wavelength ($I_{\lambda 2}$), by means of an inversion algorithm that makes use of a set a precomputed lookup tables (LUTs) of radiances emerging at the top of an aerosol-laden atmosphere. This retrieval approach is also referred to as the ''direct method'' (Torres et al. 1998).

a. Retrieved parameters

Since only two independent pieces of information are available from the TOMS observations (i.e., radiances at two near-UV channels), two aerosol related parameters can be retrieved, and assumptions must be made about the others. The retrieved quantities are aerosol extinction optical depth and a microphysical aerosol property. The choice of the second retrieved quantity depends on the aerosol type. In the TOMS aerosol retrieval algorithm, it is assumed that the variability (both spatial and temporal) of dust aerosol particle size is larger than the variability of its composition (i.e., refractive index). Therefore, when it is assumed that the aerosol type is mineral dust, the second retrieved parameter is the effective particle size. In the case of carbonaceous particles, it is assumed that the time and space variability of the aerosol composition is larger than the particle size variability. Thus, if the observed aerosol type is carbonaceous, the second retrieved parameter is the imaginary component of the refractive index. Torres et al. (1998) discuss the rationale of the assumptions regarding temporal and spatial variability of aerosol microphysical properties. The single scattering albedo associated with the retrieved microphysical property (and the assumed values for the others) is calculated.

TABLE 1. Aerosol models.

Aerosol model		Size distribution			Complex refractive index				
		r_0	σ	r_{eff}	331 nm	340 nm	360 nm	380 nm	550 nm
Sulfate	S	0.07	2.03	0.24	1.43–0*i*	1.43–0*i*	1.43–0*i*	1.43–0*i*	1.43–0*i*
Carbon 1	C1	0.08	1.45	0.10	1.55–0.0150*i*	1.55–0.150*i*	1.55–0.150*i*	1.55–0.150*i*	1.55–0.0150*i*
Carbon 2	C2	0.08	1.45	0.10	1.55–0.0350*i*	1.55–0.350*i*	1.55–0.350*i*	1.55–0.350*i*	1.55–0.0350*i*
Carbon 3	C3	0.08	1.45	010	1.55–0.0550*i*	1.55–0.550*i*	1.55–0.550*i*	1.55–0.550*i*	1.55–0.0550*i*
Dust 1	D1	0.07	1.95	0.21	1.58–0.0207*i*	1.58–0.0196*i*	1.57–0.0175*i*	1.58–0.0150*i*	1.56–0.0060*i*
Dust 1a	D1a	0.12	2.20	0.57	1.58–0.0207*i*	1.58–0.0196*i*	1.57–0.0175*i*	1.58–0.0150*i*	1.56–0.0060*i*
Dust 2	D2	0.25	2.20	1.13	1.58–0.0207*i*	1.58–0.0196*i*	1.57–0.0175*i*	1.58–0.0150*i*	1.56–0.0060*i*
Dust 3	D3	0.50	2.20	2.26	1.58–0.0207*i*	1.58–0.0196*i*	1.57–0.0175*i*	1.58–0.0150*i*	1.56–0.0060*i*

b. Sensitivity analysis

Under cloud-free conditions the accuracy of the retrieved parameters is determined mainly from the errors in the prescribed surface reflectivity and aerosol layer height. For the sake of completeness, a brief summary of a previously published analysis of errors in retrieved optical depth [Table 3 of Torres et al. (1998)] is included here.

For a surface reflectivity uncertainty of ± 0.01 the accuracy of the retrieved optical depth is ± 0.1 for nonabsorbing and weakly absorbing aerosols. As the aerosol becomes more absorbing, the sensitivity to surface albedo decreases, and the accuracy of the retrieval is better than ± 0.05. An uncertainty of ± 1 km in the prescribed aerosol layer height produces negligible optical depth errors ($\pm 2\%$) in the case of nonabsorbing aerosols. However, as aerosol absorption increases, so does the altitude error in optical depth, which may be as large as 65% for strongly absorbing aerosols. The optical depth is overestimated when the prescribed aerosol layer height is lower than the actual value. When the assumed aerosol location is higher than the actual value, an optical depth underestimate takes place. The optical depth sensitivity to aerosol location is asymmetric; that is, larger errors result when the aerosol layer height is underestimated. Subpixel cloud contamination is an additional source of error that produces aerosol optical depth overestimates. Based on this error analysis, it is estimated that the achievable accuracy in retrieved optical depth using the near-UV technique is the largest of 0.1 or 20% for nonabsorbing aerosols (due to uncertainty in prescribed surface albedo and subpixel cloud contamination). The estimated uncertainty for most cases of UV-absorbing aerosols is about 30%. This estimate correspond to moderately absorbing aerosols [models C1, C2, and D1 in Table 3 of Torres et al. (1998)]. The more absorbing D2 and D3 types used in the previously published sensitivity analysis are only seldom observed nearby their sources during the occurrence of dust storms. The large errors associated with the retrieval of these extreme events are not representative of the performance of the retrieval procedure under most conditions.

c. Aerosol models

Three major aerosol types are used to describe the tropospheric aerosol load: sulfate aerosols, carbonaceous particulate, and mineral aerosols. The selected aerosol models are representative of the most commonly observed aerosol types. The microphysical properties of the aerosol models at the TOMS near-UV wavelengths (331, 340, 360, and 380 nm) are summarized in Table 1 and are based on measurements. Values of aerosol microphysical properties at a standard visible wavelength (550 nm) are also included as a reference. Note that the assumed refractive index of the carbonaceous aerosol models is wavelength independent, whereas the imaginary component of the refractive index for the mineral dust aerosol models is spectrally dependent, even in the narrow near-UV range (Patterson et al. 1977; Sokolik et al. 1993). Some of the aerosol models used in the previously published sensitivity analysis (Torres et al. 1998) have been revisited to incorporate new information on aerosol particle size distributions. Model S remains unchanged, new particle size distributions for models C1 and C2 are used. In addition, a more absorbing carbonaceous aerosol model (C3) was added. Finally, an additional dust model labeled (D1a) has been introduced. The concentration of sulfate (S) aerosol type has a maximum at the surface and decreases exponentially with altitude. The UV-absorbing aerosols are assumed to be concentrated in a single layer above surface level and represented by a Gaussian distribution. The precomputed LUTs are separated in two sets: a dust–sulfate (DS) lookup table (one sulfate and four mineral dust aerosol models), and a carbonaceous–sulfate (CS) lookup table (one sulfate and three carbonaceous aerosol models). Note that none of the aerosol models are assumed to exactly represent the actual atmospheric aerosol type. Instead, they are nodal points upon which interpolation between different aerosol models is carried out.

In the retrieval algorithm the choice of aerosol lookup table (either CS or DS) is based on a combination of factors. A database on surface scene type compiled by the Clouds and the Earth's Radiant Energy System (CERES) project is used for retrievals over land. The DS array of models is chosen when the underlying scene

type is characterized as an arid or semiarid environment. The CS family of model is selected for all other land types. Over the oceans, aerosol type is directly specified. In general, the CS array is prescribed over the Southern Hemisphere oceans, and the DS array over the Northern Hemisphere, except over specific geographic regions where carbonaceous aerosols are the most likely aerosol type present (i.e., South China Sea and oceanic regions in the vicinity of Central America). Since the retrieval approach does not consider mixtures of mineral and carbonaceous aerosols, retrieval errors are likely to take place in the Sahelian region where dust–smoke mixtures are possible in Northern Hemisphere winter.

d. Environmental model

Surface albedo values in the near UV are selected based on an existing climatogy of minimum TOMS measured reflectivity over the lifetime of the *Nimbus-7* TOMS instrument (Herman and Celarier 1997).

The height of the absorbing aerosol layer is assumed to be 3 km for carbonaceous aerosols. For mineral dust, the aerosol layer height has been taken from a climatology of monthly mean values using calculations from the chemical transport model of Ginoux et al. (2001). The use of monthly mean values is based on the assumption that the interannual variability of aerosol height is of secondary importance, which is consistent with the findings of Cakmur et al. (2001). The aerosol layer height on a given day is estimated by linear interpolation using the corresponding two monthly mean values. Since the daily variability of the aerosol vertical distribution is not accurately accounted for, the aerosol layer height assumption remains a source of uncertainty in the TOMS aerosol products.

Pixel-size cloud effects are easily excluded by rejecting data for pixels with reflectivity larger than 15%. To screen out those scenes where subpixel cloud contamination may be significant, an additional constraint on the reflectivity is imposed making use of the Aerosol Index. In general, pixels with reflectivities larger than 0.1 are used for aerosol retrieval as long as the absolute value of AI is larger than a threshold value. This approach is based on the fact the AI approaches zero for clear scenes and in the presence of clouds.

Sun glint effects are excluded by rejecting those observations when the viewing geometry over the oceans favors sun glint occurrence. The possible effect of clear water absorption in the near-UV (Litjens et al. 1999) is also screened out by rejecting data over the open oceans where the aerosol index is smaller than about 0.6. This effect could generate a spectral signal in the near-UV, similar to that of absorbing aerosols. A correction method is currently under development.

4. Application of near-UV method to TOMS observations

a. The TOMS record

The near-UV aerosol retrieval method has been applied to the multiyear record of backscattered ultraviolet radiance observations. The original TOMS sensor was primarily conceived to retrieve atmospheric column ozone amount. The record of backscattered UV radiances started in October 1978 with measurements by the TOMS sensor on board the *Nimbus-7* satellite and extended continuously until April 1993. A second sensor on the Russian *Meteor3* spacecraft operated between August 1991 and December 1994. After an 18-month gap, the TOMS record continued with the launch of two new sensors on board the *Earth Probe* (*EP*) and *Advanced Earth Observing Satellite* (*ADEOS*) satellites (7 months of operation until the spacecraft failure in 1997). The *EP*-TOMS sensor is currently operating. The *Nimbus-7*- and *Meteor3*-TOMS sensors measured backscattered radiances at six wavelengths in the range 312–380 nm while the newer instruments make measurements in the 308–360-nm range. Measurements in the 331–380-nm range, where gaseous absorption is negligible are used to derive aerosol properties by the method discussed in this paper. Although the retrieval is done using two different pairs of wavelengths depending on the instrument (i.e., 340–380 nm for *Nimbus-7* and *Meteor3*, and 331–360 nm for the others), the results are reported at 380 nm for continuity of the longer (1978–93) *Nimbus-7*-TOMS record. The retrieval algorithm is applied to the orbital or level-2 TOMS data. The level-2 data spatial resolution at nadir is about 50×50 km^2 for the *Nimbus-7* and *Meteor3* sensors, and about 40×40 km^2 for the others. The footprint size increases with increasing satellite zenith angle, reaching values as high as 200×200 km^2. Retrieved products are gridded at a $1^\circ \times 1^\circ$ resolution to produce daily, weekly, and monthly averages. To facilitate the intercomparison with other global aerosol products (i.e., AVHRR, MODIS), visible optical depth and single scattering albedo products are created by converting the derived near-UV parameters to 550 nm. The conversion is carried out using the theoretically established spectral dependence associated with the adopted aerosol models optical properties (see Table 1). Sample retrievals of optical depth and single scattering albedo for specific events have been published elsewhere (Torres et al. 2001). A validation analysis of the single scattering albedo product, is currently under way and will be published separately.

b. Optical depth validation

1) THE AERONET DATABASE

AERONET, a federated network of CIMEL sun photometers (Holben et al. 1998), measures spectral aerosol optical depths (Eck et al. 1999) every 15 min from direct

TABLE 2. AERONET sun photometer sites used in this study.

AERONET site	Lat, long	Location	Aerosol type	Period
GSFC	39°N, 77°W	Maryland	Industrial	1996–2000
CART	37°N, 97°W	Oklahoma	Industrial	1996–2000
Bondville	40°N, 88°W	Illinois	Industrial	1996–2000
Mongu	15°S, 23°E	Zambia	Smoke	1996–2000
Banizoumbou	14°N, 3°E	Niger	Dust/smoke	1996–2000
Bidi-Bahn	14°N, 2°W	Niger	Dust/smoke	1996

sun measurements at 8 wavelengths (340, 380, 440, 500, 670, 870, 940, and 1020 nm), except for a few sites in northern Africa where the shortest wavelength available is 440 nm. Aerosol particle size distribution and refractive index (both real and imaginary components) are also derived from sky radiance measurements (Dubovik and King 2000). These measurements are carried out at a large number of sites around the world. Because of the availability of aerosol optical depths at near-UV wavelengths, and the diversity of environments covered, which allows the ground–satellite comparisons for different conditions of atmospheric aerosol load, this is a valuable dataset for the validation of the TOMS aerosol optical depth. Although AERONET currently consists of over one hundred stations worldwide, only a few sites have continuous records over a full year or longer. Unfortunately, no AERONET data are available to validate the TOMS data prior to May 1993.

In this section, a comparison of the *EP*-TOMS aerosol optical depth to AERONET sunphotomer measurements is carried out at a variety of sites characterized by different types of atmospheric aerosols. In order to validate the TOMS retrieval under different aerosol load conditions we have selected six sites in regions, each characterized by one of the three most predominant tropospheric aerosol types: sulfate, carbonaceous and mineral aerosols, and with long enough records to allow comparisons along the seasonal aerosol cycle. Table 2 lists the AERONET sites used in the analysis. Except for the Banizoumbou and Bidi-Bahn sites, the satellite–ground comparisons were made at 380 nm. At the dust sites the comparison was made at 440 nm, which is the shortest wavelength available. The average of the *EP*-TOMS measurements within a $1° \times 1°$ box centered at the AERONET site, are compared to the average of the sun photometer observations within 30 min of the satellite overpass. Correlation coefficients and the parameters of the resulting AERONET–TOMS linear fit are shown in Table 3.

2) NONABSORBING AEROSOLS

A comparison of satellite derived optical depths of nonabsorbing aerosols to AERONET observations at three locations in the continental United States [GSFC, Cloud and Radiation Testbed (CART), and Bondville] are shown in Fig. 1. The dotted lines above and below the one-to-one line in Figs. 1a, 1b, and 1c indicate the largest of 0.1 optical depth, or 20% departure from the ground-based measurement. The resulting linear fit between the AERONET and TOMS observations is also shown. Largest *EP*-TOMS overestimations occur at optical depth values lower than about $\tau = 0.2$. This overestimation underscores the disadvantage of the large *EP*-TOMS FOV that prevents the separation of aerosol effects from those of optically thin clouds. For sunphotometer measured values larger than about $\tau = 0.2$, the level of agreement is within the predicted accuracy based on the uncertainties associated with the prescribed values of surface albedo and subpixel cloud contamination. The resulting correlation between the ground and space measurements (0.70 at GSFC, 0.84 at the CART site, and 0.58 at Bondville) is mainly driven by those retrievals larger than $\tau = 0.3$. If only retrieved values lower than $\tau = 0.3$ are used, the resulting correlation loses statistical significance.

3) ABSORBING AEROSOLS

EP-TOMS retrieved values of UV-absorbing aerosol optical depths are compared to ground-based measurements at three AERONET sites: Mongu, Banizoumbou,

TABLE 3. Summary of comparison results.

Site	Total points	Percent within uncertainty	Correlation coefficient	Linear fit		Std dev	
				Y intercept	Slope	*Y* intercept	Slope
GSFC	164	78	0.700	0.089	0.629	0.011	0.050
CART	51	72	0.838	0.085	0.766	0.016	0.071
Bondville	99	85	0.584	0.135	0.453	0.017	0.064
Mongu	32	65	0.966	0.067	0.997	0.047	0.049
Banizoumbou	98	64	0.830	0.095	0.844	0.034	0.058
Bidi-Bahn	52	62	0.815	0.086	0.752	0.042	0.076
All	496	74	0.890	0.058	0.884	0.009	0.020

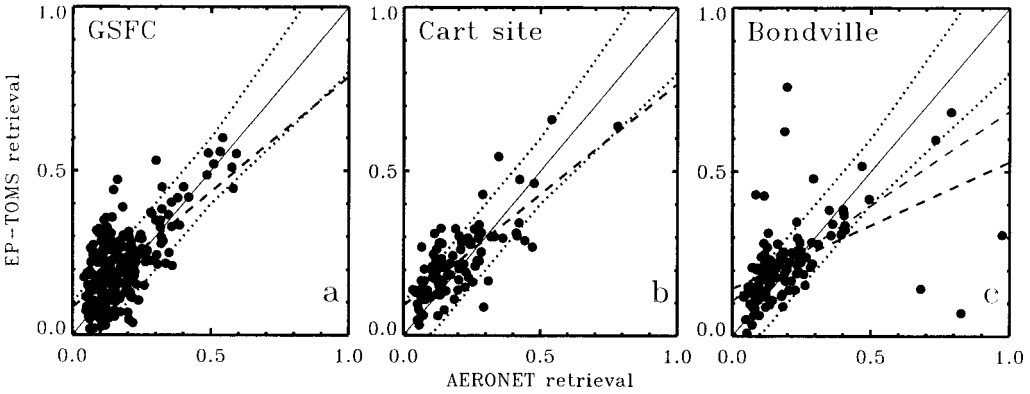

FIG. 1. Comparison of *EP*-TOMS retrieved optical depth for nonabsorbing aerosols to AERONET measurements at (a) Goddard Space Flight Center, (b) CART site, and (c) Bondville. The one-to-one agreement is indicated by the solid line. Dashed lines represent the predicted uncertainty of the satellite retrieval for nonabsorbing aerosols (larger of 0.1 and 20%). The thick dashed line is the resulting linear fit.

and Bidi-Bahn. The comparison in Mongu is done at 380 nm. For the Banizoumbou and Bidi-Bahn comparisons, measurements at the shortest wavelength available, 440 nm, were used. Scatterplots in Figs. 2a, 2b, and 2c depict the level of agreement between the two datasets. Dashed lines indicate the expected uncertainty associated with prescribed values of surface albedo, aerosol layer height, and subpixel cloud contamination (Torres et al. 1998). Carbonaceous particles produced by intense biomass burning are the predominant aerosol type in southern Africa (Zambia) where Mongu is situated. The aerosol type at Banizoumbou and Bidi-Bahn in the Sahel region varies markedly around the year. In winter and early spring the aerosol load is a mixture of carbonaceous aerosols from biomass-burning activities and mineral dust flowing south from the Lake Chad area and other sources. During the fall and summer seasons, the atmospheric aerosol load is primarily made up of mineral dust. As shown in the corresponding scatterplots (Figs. 2b and 2c), the *EP*-TOMS retrieved optical depth compares reasonably well to the AERONET measurements with most of the data within the theoretically predicted uncertainty. The resulting correlation coefficients are 0.97 (at Mongu), 0.82 (at Bidi-Bahn), and 0.83 (at Banizoumbou).

4) DISCUSSION

A summary of the validation analysis of the TOMS aerosol optical depth is shown in Table 3. The percentage of retrievals within the expected uncertainty range is larger for scattering-only aerosols than for absorbing aerosol types as shown in the third column of Table 3. The larger TOMS frequency of departure from the ground-based observations at the absorbing aerosol sites is explained by the sensitivity to aerosol height. Most of the points out of the range of expected uncertainty are overestimates when the AERONET measured optical depth is less than about 0.3. This feature of the TOMS validation analysis underscores the difficulty in removing low levels of subpixel cloud contamination in the retrieval process. Most departures from the expected accuracy when the ground measured optical depth value is larger than about 0.4, take place at the

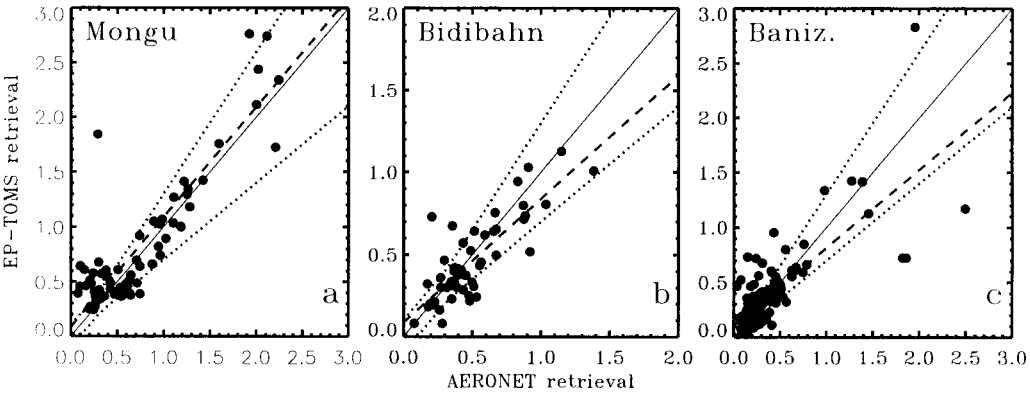

FIG. 2. As in Fig. 1 for absorbing aerosols at (a) Mongu, (b) Bidi-Bahn, and (c) Banizoumbou. Dashed lines represent the predicted uncertainty of the satellite retrieval for absorbing aerosols (larger of 0.1 and 30%).

absorbing aerosol sites, probably due to errors in the prescribed aerosol layer height.

The statistically meaningful correlation coefficients obtained in the TOMS–AERONET analysis (Table 3, column 4) are mainly the result of the good agreement between the measurements when the 380 nm optical depth is larger than about $\tau = 0.3$. When the comparison is restricted to those days when the AERONET measured optical depth was less than $\tau = 0.3$ the resulting correlation coefficients are not statistically meaningful at four out of the six sites in this analysis. Possible physically based reasons for the TOMS apparent loss of sensitivity to low aerosol amounts include errors in prescribed surface reflectivity, unaccounted for Rayleigh scattering effects (i.e., residual errors in molecular scattering coefficients), and radiance contamination effects due to subpixel size clouds and/or optically thin cirrus clouds. Any of the first two effects would produce a nearly constant bias in the TOMS retrieval with respect to the AERONET measurement. Based on the random distribution of the TOMS–AERONET differences, however, errors in prescribed surface reflectivity or molecular scattering coefficients are not likely to explain the obtained poor correlation. Given the large TOMS footprint, cloud contamination is a significant error source in the TOMS retrieved optical depth. Errors due solely to subpixel cloud contamination, however, will consist of a systematic optical depth overestimation. Since the distribution of overestimates and underestimates (within the ranges of expected accuracy) is random, subpixel cloud contamination (or thin cirrus effects) alone does not explain the AERONET–TOMS discrepancy when the optical depths are small. A plausible explanation of the scatter of the TOMS retrieved optical depth around the AERONET values may be related to sampling. The TOMS retrieval is an average over a $1^\circ \times 1^\circ$ box, while the AERONET observation is a point measurement. If the spatial variability of the atmospheric aerosol load is significant, a point measurement may not be representative of the large-area-average optical depth reported by the TOMS retrieval method. The parameters of the linear fits in Figs. 1 and 2 and their standard deviations are listed in columns 5 and 6 of Table 3. The comparison of TOMS derived optical depths to AERONET measurements indicates that in spite of the instrumental limitations (i.e., unsuitable spatial resolution for aerosol retrieval), the near-UV method to retrieve aerosol optical depth over land surfaces works reasonably well. The degree of correlation and average agreement over several measurements indicates that the two methods are equivalent for their differing FOVs. A total of 496 coincident measurements were used in this analysis. Of these, 314 events corresponded to nonabsorbing aerosols while the reminder 182 cases corresponded to either mineral, carbonaceous or mixtures thereof. In about 75% of the 496 coincident measurements, the AERONET–TOMS difference is within the predicted uncertainty. The level of agreement increases to 80% if only nonabsorbing aerosols are considered, and decreases to about 70% for absorbing aerosols. The better performance of the near-UV method in the retrieval of nonabsorbing aerosol optical depth is due to the insensitivity to the aerosol vertical distribution.

The main source of error is the presence of subpixel cloud contamination. For absorbing aerosols, on the other hand, the departure from the ground-based observations is due to the combined effect of uncertainty in the prescribed aerosol layer height and subpixel cloud contamination. The subpixel cloud effect is not a big source of error in the retrieval of optical depths of mineral dust layers in areas not too far from their sources where meteorological conditions do not favor cloud formation. Both subpixel cloud contamination and uncertainty in aerosol layer height are equally important error sources in the characterization of carbonaceous aerosols. Aerosol height uncertainty becomes an increasingly important source of error as the smoke layer rises into the free troposphere to be transported thousands of kilometers away. Under these conditions, the assumption of a single aerosol layer height as prescribed in the retrieval breaks down. For detailed regional retrievals, the variation in plume height can be incorporated as part of the retrieval algorithm.

5. TOMS aerosol optical depth record

a. Global climatology

The near-UV technique of aerosol properties retrieval has been applied to the *Nimbus-7* (January 1979–April 1993) and *Earth Probe* (July 1996–December 2000) TOMS record of near-UV radiances. Figure 3 shows the time series of global zonally and weekly averaged near-UV optical depths over the years of operation of the two sensors. The 1° longitudinal average was done requiring that at least 10% of zonal coverage was available per week. The obtained time series shows the seasonal cycle of mineral dust aerosols in the Northern Hemisphere and carbonaceous aerosols in the Southern Hemisphere. The effects of the two major volcanic eruptions of the last 20 years (El Chichón 1982; Mt. Pinatubo 1991) clearly show in the TOMS aerosol optical depth record. A 6-week gap in mid-1990 was produced by temporary instrumental difficulties.

Figure 4 shows global maps of the long-term monthly average aerosol optical depth over the 13-yr period (1979–91) from *Nimbus-7*-TOMS observations. The geographical resolution is $1^\circ \times 1^\circ$. Given the loss of spatial coverage due to clouds and snow–ice interference, we have applied a restriction in the averaging procedure to ensure that the reported monthly mean values are representative of the long-term record. Only pixels with at least three observations in any given month over the entire 13-yr record were used to calculate the average value shown on the monthly maps. The largest loss of spatial coverage is observed north

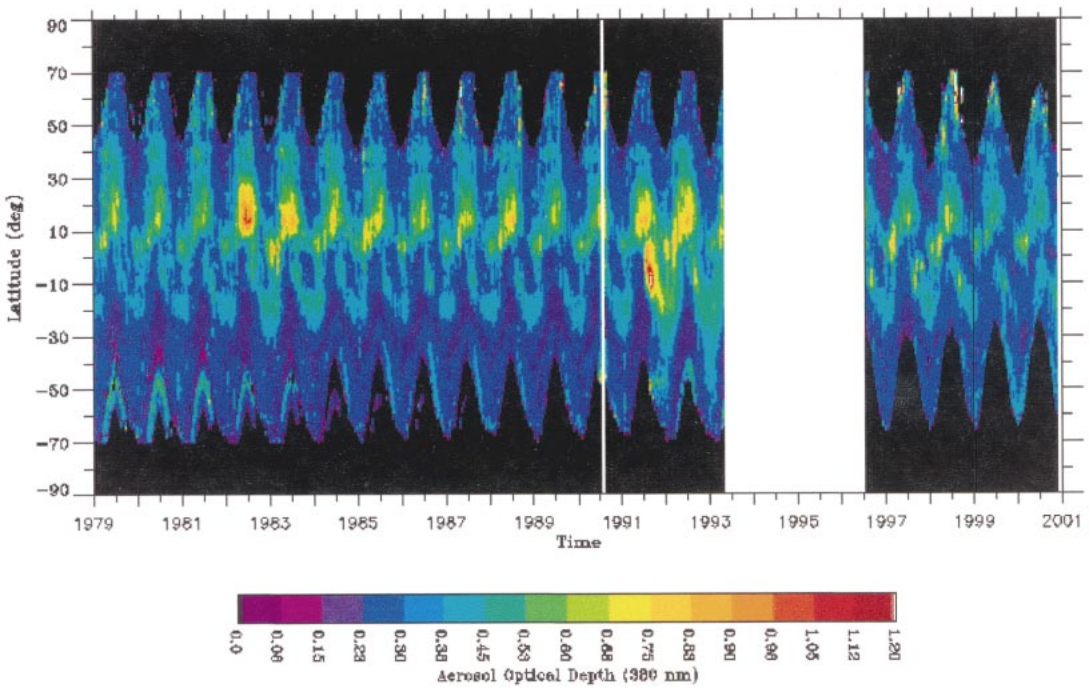

FIG. 3. Time series of the zonally averaged 380-nm aerosol optical depth over the period of operation of the TOMS instruments on board the *Nimbus-7* (1979–92) and *Earth Probe* satellites (1996–present). Weekly averages over a $1° \times 1°$ geographical grid are plotted.

of about 35°N in winter (January through March) produced by the persistent presence of clouds at midlatitudes and both clouds and snow cover at high latitudes (Herman et al. 2001). The Southern Hemisphere loss of spatial coverage in winter is smaller than in the Northern Hemisphere.

The obtained climatology clearly illustrates the sources and spatial distribution patterns of the most predominant aerosol types. From November to March, large aerosol amounts (average optical depth larger than 1 near the source regions) are generated by biomass-burning activities in sub-Sahelian region. The dense smoke plume spreads over the Atlantic Ocean in a region from about 10°S to 10°N. The Northern Hemisphere component of this aerosol plume in February is enhanced by the outset of Saharan dust flow. The spring months are characterized by intense Saharan dust outbreaks when large amounts of dust are transported over the Mediterranean and the Middle East. During April–June aerosols are intensively generated in the Northern Hemisphere while the Southern Hemisphere is relatively free of anthropogenic aerosols with an average value of about 0.3 over the oceans and even smaller (less than 0.2) over the remote continental regions of South America, South Africa, and Australia. The beginning of the Northern Hemisphere biomass-burning season takes place in March–April in Central America, Southeast Asia, and China. The Central American smoke plume spreads both west over the Pacific Ocean and northwest covering a vast area of the western United States. The most prominent aerosol feature in June, July, and August is the almost continuous easterly flow of dust from northern Africa across the Atlantic Ocean. Intense dust flow activity is also observed over other well-known arid areas: Arabian Peninsula, northern India, etc. The presence of a horizontally extended and optically thick aerosol layer produced by forest fires is observed during July, August, and September over eastern Russia. September and October mark the onset of the dust season. The intense Southern Hemisphere biomass-burning season starts in July in Central Africa. The smoke plume from these fires is a persistent feature from July to December. The peak of the biomass-burning season in South America takes place in August and September.

b. Regional climatologies

Carbonaceous and mineral dust particles are by far the most predominant tropospheric aerosol types. The global frequency of occurrence of UV-absorbing aerosols has been previously discussed in terms of the TOMS aerosol index (Herman et al. 1997). The highest concentrations of carbonaceous and mineral dust aerosols are found in the vicinity of their source regions frequently located in remote areas. Because of the known difficulties of measuring aerosols from space over land surfaces using visible and near-IR observations, long-term satellite records of aerosol optical depth over land did not exist until the development of the near-UV method of aerosol sensing. In this section we

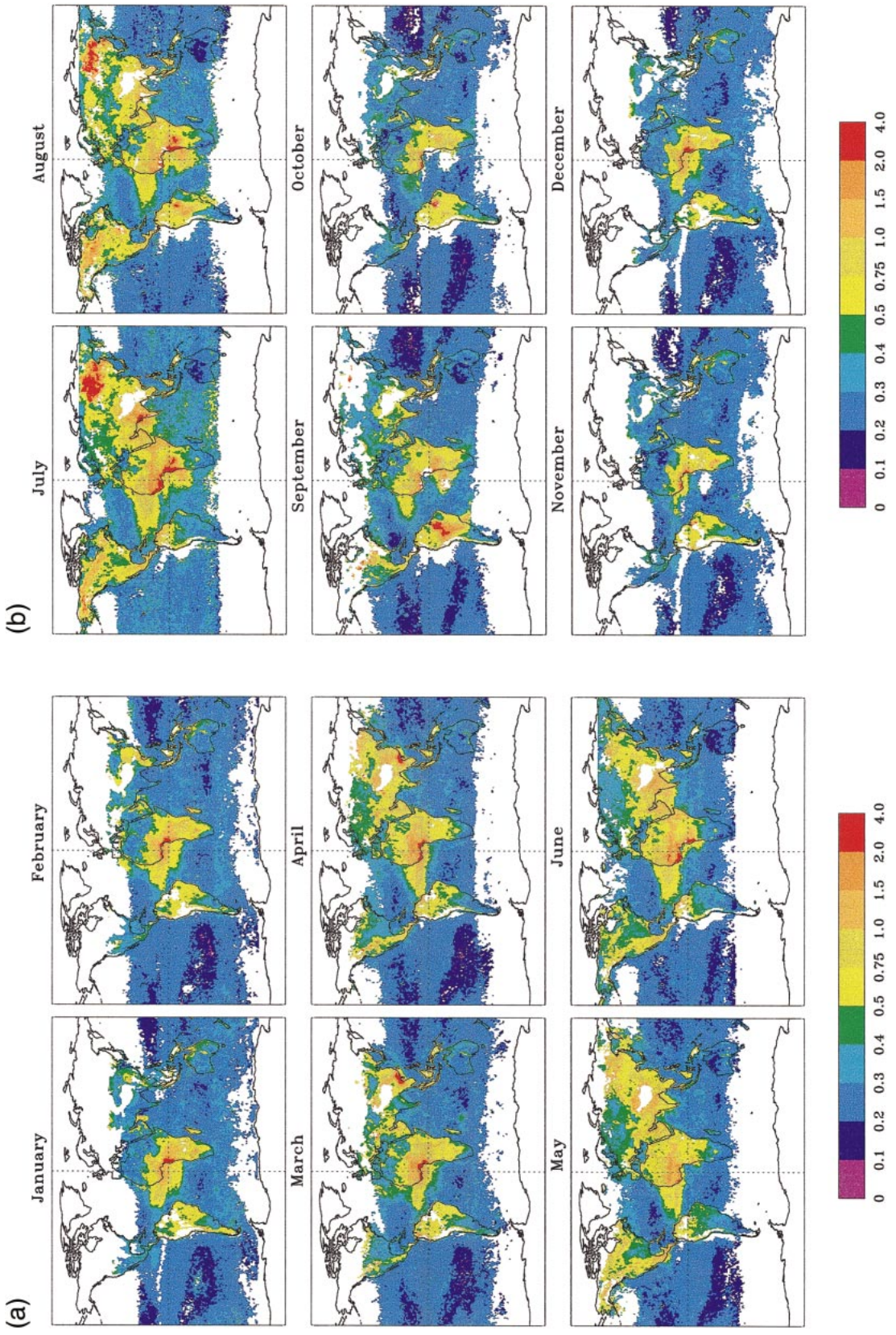

FIG. 4. Long-term (1979–91) global monthly average aerosol optical depth derived from *Nimbus-7*-TOMS observations.

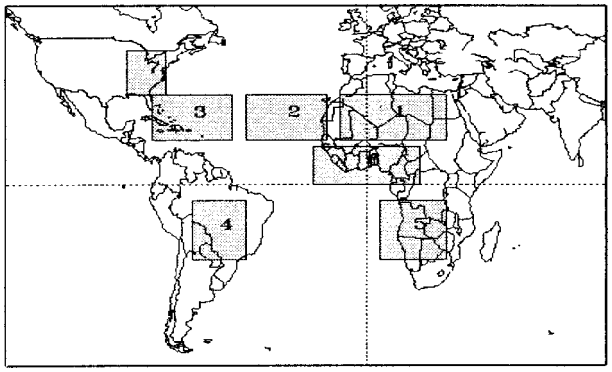

FIG. 5. Selected world areas for regional climatology analysis: Saharan Desert, eastern Atlantic Ocean, western Atlantic Ocean, Sahel region, southern Africa, southern Brazil, and eastern United States.

briefly discuss the temporal evolution of the atmospheric aerosol load over the regions shown in Fig. 5: Saharan Desert (15°–30°N, 10°W–30°E), eastern Atlantic Ocean (15°–30°N, 15°–45°W), western Atlantic Ocean (15°–30°N, 50°–80°W), Sahelian region (0°–13°N, 20°W–20°E), southern Africa (5°–25°S, 5°–30°E), South America (5°–25°S, 45°–65°W), and eastern United States (30°–45°N, 75°–90°W). The regional climatologies discussed here cover the 14-yr (1979–92) record of aerosol optical depth derived from observations by the *Nimbus-7* TOMS sensor. Only grid points with at least 5 days of data in a month were included in the calculations.

1) SAHARAN DESERT AND ATLANTIC OCEAN

The long-term record of aerosol load over the Saharan Desert and Atlantic Ocean and the mean annual cycle over the lifetime of the *Nimbus-7* TOMS sensor are depicted in Figs. 6, 7, and 8. Over the Saharan Desert (Fig. 6a), a well-defined annual cycle is observed, with minimum ($\tau = 0.25$) optical depth values during the winter months followed by a rapid rise during the spring season. The March–August months are characterized by high aerosol load with the annual peak values of about $\tau = 0.75$ occurring in the May–July period. The absolute maximum in May of 1982, followed by a rapid decay in 1983 and 1984 is due to the added contribution of the stratospheric aerosol layer formed as a result of the El Chichón eruption in April 1982. A return to the pre-eruption maximum of about $\tau = 0.75$ is observed in 1986. The years 1987 and 1988 show unusually high values (larger than 0.8) that cannot be explained by any significant volcanic activity, followed by 2 years (1989 and 1990) with lower summer peak values. The large optical depth values in the spring of 1991, with a sharp May peak (before the June 1991 Mt. Pinatubo eruption) may have been produced by the spillover effects over the eastern Saharan of the short lived optically thick tropospheric aerosol layer that resulted from the burning of oil during the 1991 Persian Gulf War. The high 1992 summer peak in excess of $\tau = 0.8$ may contain a contribution from the effects of the stratospheric aerosol layer after the Mt. Pinatubo eruption. There appears to be a small increase in the background aerosol load from a minimum of about $\tau = 0.25$ in the early 1980s to about $\tau = 0.3$ in the late 1980s and early 1990s.

Figures 7 and 8 show the influence of the Saharan dust westward transport on the aerosol load over the Atlantic Ocean. Although, as expected, the eastern Atlantic Ocean region (Fig. 7) shows a similar seasonality as the Sahara itself, a few interesting features are worth mentioning. A 1-month lag is observed in the summer maximum over the east Atlantic. The winter background value of about $\tau = 0.3$ is larger than its counterpart over the desert itself. The eastern Atlantic background values shows a much smaller variability in the multiyear record than the one observed over the Saharan region. A distinct feature over the eastern Atlantic is the occurrence of a secondary winter maximum. It is interesting to note that the years 1988 and 1989 are particularly anomalous with respect to the repeatability of the annual cycle. The extraordinarily large peak in the summer of 1988 is followed by an unusually pronounced

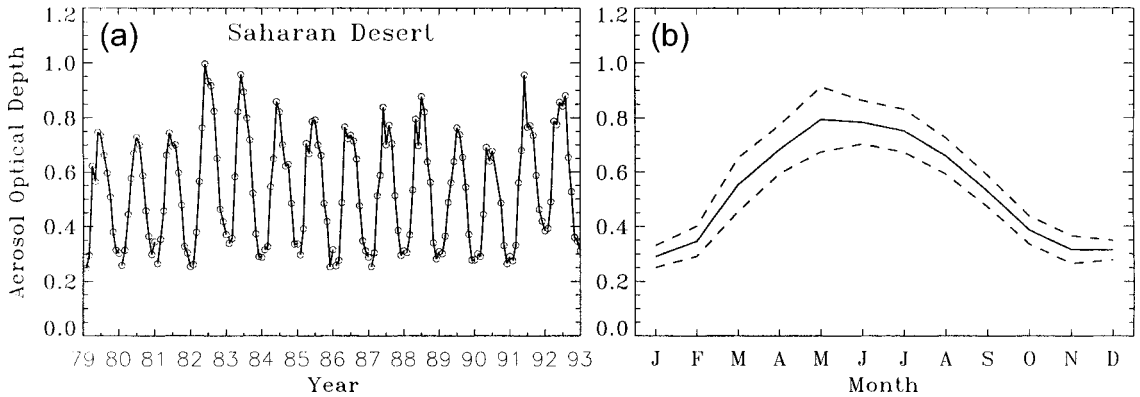

FIG. 6. (a) Time series of monthly averaged aerosol optical depth for the 1979–92 period for the Saharan Desert, (b) mean annual cycle (solid line) and std dev (dashed lines) over the period of the analysis.

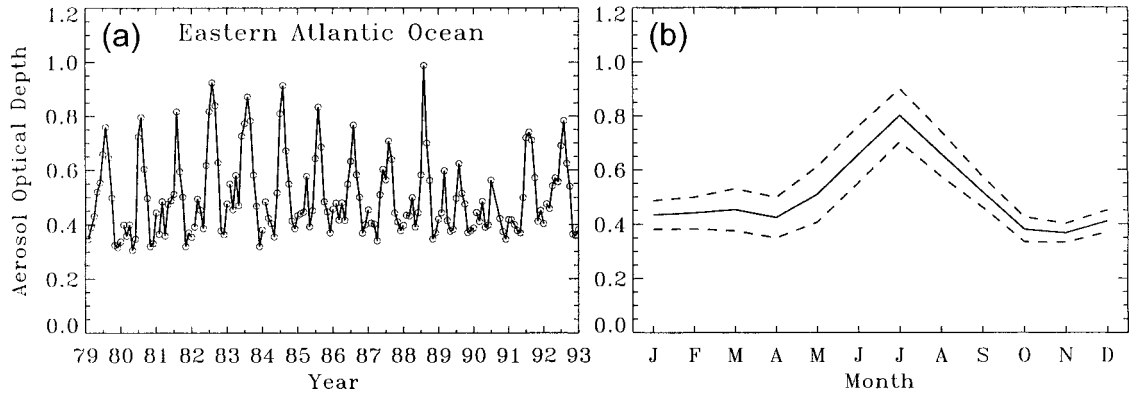

FIG. 7. As in Fig. 6 for the eastern Atlantic Ocean.

winter maximum (about twice as large as in previous years) and a particularly low summer peak in 1989. Significantly smaller optical depth values are observed over the western Atlantic Ocean region (Fig. 8). The effects of the El Chichón and Mt. Pinatubo eruptions are observed and the summer and winter peaks are clearly defined. The western Atlantic Ocean background in the fall season remains remarkably constant at about $\tau = 0.3$ during the entire 14-yr period.

2) BIOMASS-BURNING REGIONS

Figures 9, 10, and 11 illustrate the long-term record of aerosol optical depth over the three major regions of the world where seasonal biomass burning is known to be a long-established agriculture related practice. The climatology of aerosol optical depth shows similar seasonality in South America (Fig. 9) and southern Africa (Fig. 10), obeying the precipitation patterns common to the two areas. Minimum optical depth values (about $\tau = 0.25$) are observed in the June–July period in South America. Slightly larger values are observed in southern Africa in the April–June period. The biomass-burning season in South America is only about 3 months long with peak optical depth values in August and September. There is considerable interannual variability in the optical depth maximum. Monthly average values larger than 1.0 were recorded in 1981, 1985, 1987, 1988, and 1991, whereas in 1989 and 1990 peak values of less than about $\tau = 0.5$ were observed. Although the overall maximum optical depth in southern Africa is also recorded in the months of August and September, the biomass-burning season extends through the end of the year. A lot less interannual variability is observed with peak values between $\tau = 0.6$ and $\tau = 0.8$ during most years. The high 1991 and 1992 values are possibly affected by the Mt. Pinatubo eruption.

The time series of optical depth over the Sahel region in central Africa is shown in Fig. 11. The biomass-burning season in this part of the world, starts in the November–December period and extends for several months until March–April. Although significant biomass burning takes place in this area early in the year, the high optical depth amounts retrieved by TOMS are very likely the result of the combined effect of carbonaceous particulate produced by the intense fire season and the southward flow of mineral dust from the ever-active Lake Chad and other significant sources of mineral dust in the Saharan Desert (Prospero et al. 2002). An average background value of about $\tau = 0.4$ is always recorded in October. Peak monthly average values generally larger than $\tau = 1.0$ are derived in spring, very

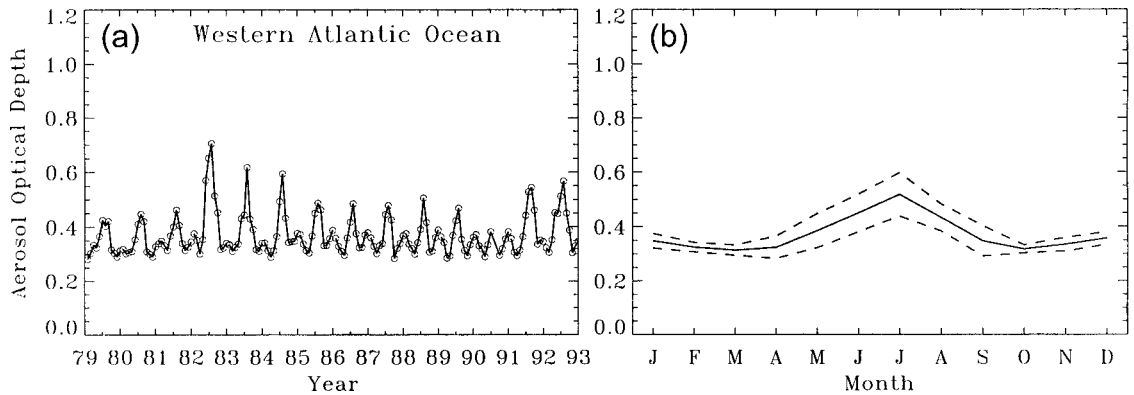

FIG. 8. As in Fig. 6 for the western Atlantic Ocean.

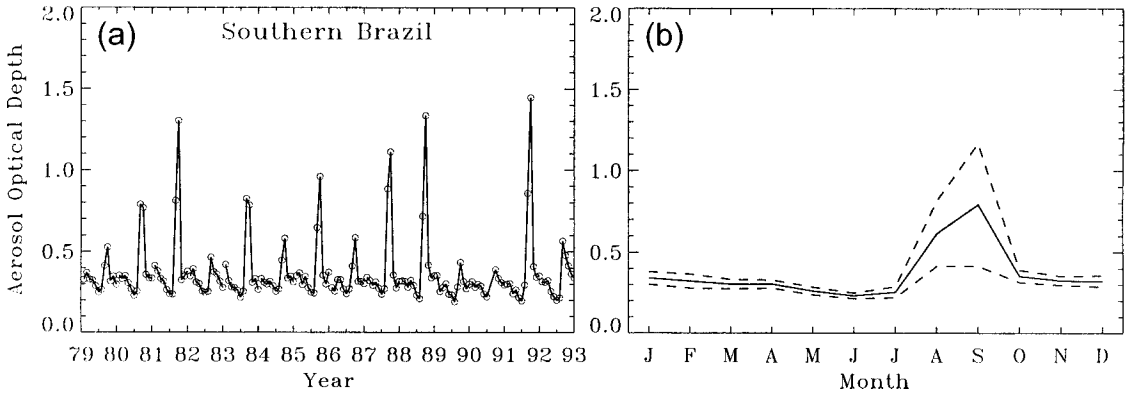

FIG. 9. As in Fig. 6 for southern Brazil.

likely resulting from the mixing of smoke and dust aerosols. According to the TOMS data, the most active years in terms of aerosol production in the Sahel region were 1983 and 1985 when the March monthly average optical depth reached a value of about $\tau = 1.7$ (0.8 at 550 nm), the highest of the 14-yr record presented here.

3) EASTERN UNITED STATES

The atmospheric aerosol load over the eastern region of the United States over the 1979–92 period, as derived from TOMS observations is shown in Fig. 12. Because of persistent interference of clouds and surface snow, not enough data are available to compute monthly averages in winter. The long-term record of aerosol optical thickness over the eastern part of the United States shows well-defined summer and fall peaks and spring minima. The sharp peaks in May 1980 and August 1981 and 1982 are the result of carbonaceous aerosols resulting from boreal forest fires and transported south by prevailing winds. The August 1982 maximum is compounded by the effects of the El Chichón eruption. The prominent peak observed in September 1988 was the result of the thick smoke layer produced by the fires that affected Yellowstone National Park that spread eastward as far as the North Atlantic Ocean. An intriguing apparent optical depth drop is observed in the last 2 years of the TOMS record over the eastern United States. Although an instrument calibration change toward the end of the lifetime of the *Nimbus-7* TOMS sensor cannot be ruled out, we feel a calibration error is not likely since the same effect is not observed in the other regional climatological analysis previously discussed.

6. Summary and conclusions

A long-term global record of aerosol optical thickness over both the oceans and the continents has been produced using observations of backscattered near-UV radiances by the TOMS sensors on board the *Nimbus-7* (1979–93) and *Earth Probe* (1996–present) satellites. The retrieval technique applied to the TOMS data, makes use of two unique advantages of near-UV remote sensing not available in the visible or near-IR. These advantages are 1) low reflectivity of all land surface types (including the normally bright deserts in the visible), which make possible aerosol retrieval over the continents, and 2) large sensitivity to aerosol types that absorb in the UV, allowing the clear separation of carbonaceous and mineral dust aerosols from purely scattering particles such as sulfate and sea salt aerosols. The

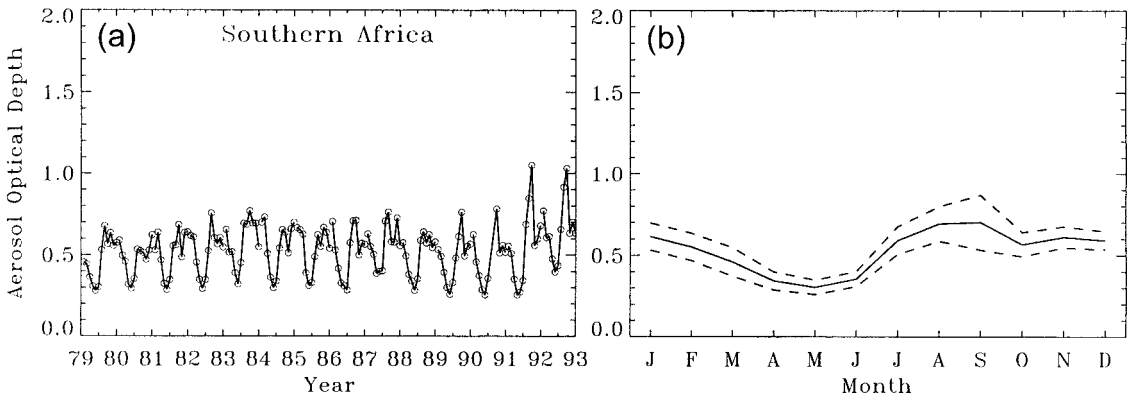

FIG. 10. As in Fig. 6 for southern Africa.

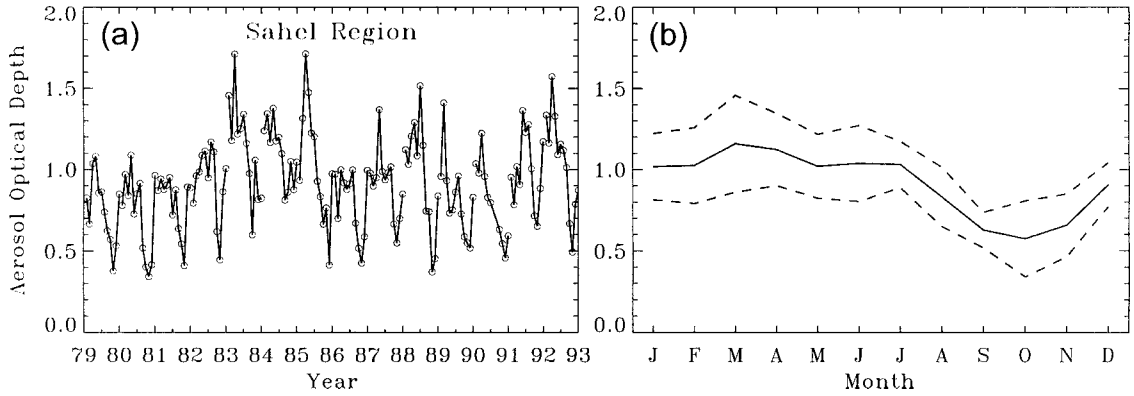

FIG. 11. As in Fig. 6 for the Sahel region.

capability to distinguish between absorbing and nonabsorbing aerosols, allows the application of a regional model approach by choosing the most likely aerosol type to predominate based on the TOMS signal and geographic location.

The accuracy of the TOMS retrieved optical depth over land was evaluated by comparing the satellite-based measurement to AERONET ground-based sun photometer observations, in environments characterized by different aerosol types such as carbonaceous aerosol from biomass burning, desert dust aerosols, and sulfate aerosols. The results of the comparison indicate that the TOMS technique works particularly well in the detection of aerosol events with optical thickness larger than about 0.2. The comparison with sun photometer for optical depths smaller than about 0.2 shows no clear correlation. We suggest that the lack of correlation, when the optical depth is small, is related to the coarse resolution of the TOMS product that makes it difficult to resolve small-scale spatial variability. In most cases the TOMS-derived optical depths of UV-absorbing aerosols are within 30% of the AERONET observations, while nonabsorbing optical depth agrees within about 20%. These results indicate that the near-UV method can be used to retrieve the optical depth of UV-absorbing and nonabsorbing aerosols rather accurately in spite of the inherent instrumental limitations.

A preliminary analysis of retrieval results shows for the first time the long-term time series of atmospheric aerosol load over land in the vicinity of the most important source areas of tropospheric aerosols such as the Saharan desert and the biomass-burning regions of Africa and South America. Even in regions of the world where carbonaceous aerosol are not frequently found, such as the eastern United States, their sporadic occurrence is easily detected by TOMS due to the large optical depth characteristic of events such the smoke layer produced by the Yellowstone National Park fire and other boreal forest burning episodes.

We intend to continue the validation of the TOMS aerosol products by systematic comparison to ground-based observations as more AERONET data become available. The validation of the TOMS single scattering albedo product is currently under way. In addition to the direct validation using observations at the ground, we plan to compare the TOMS aerosol product to other satellite-derived datasets such as MODIS (King et al. 1999) and AVHRR (Nakajima and Higurashi 1998; Mishchenko et al. 1999; Stowe et al. 1997) to learn more about the advantages and limitations of the TOMS prod-

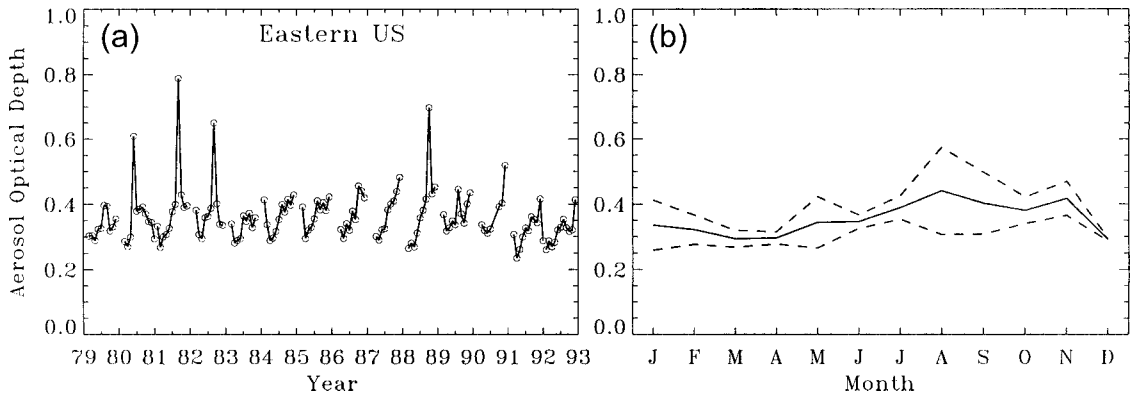

FIG. 12. As in Fig. 6 for eastern United States.

uct and improve its accuracy when possible. The TOMS aerosol climatology is available from the TOMS Web site (http://toms.gsfc.nasa.gov).

Acknowledgments. The authors would like to thank Didier Tanre from Université de Sciences et Techniques de Lille, France, for the AERONET data at the Banizoumbou and Bidi-Bahn sites used in this analysis. This work was supported in part by the NASA Global Aerosol Climatology Project (GACP) under Grant NAG5-7774. Comments and suggestions from two anonymous reviewers are gratefully acknowledged.

REFERENCES

Alpert, P., Y. J. Kaufman, Y. Shay-el, D. Tanre, A. Da Silva, and Y. H. Joseph, 1998: Dust forcing of climate inferred from correlations between dust data and model errors. *Nature,* **395,** 367–370.

Cakmur, R. V., R. L. Miller, and I. Tegen, 2001: A comparison of seasonal and interannual variability of soil dust aerosols over the Atlantic Ocean as inferred by the TOMS AI and AVHRR retrievals. *J. Geophys. Res.,* **106,** 18 287–18 303.

Dentener, F. J., G. R. Carmichael, Y. Zhang, J. Lelieveld, and P. J. Crutzen, 1996: Role of mineral aerosols surface in the global troposphere. *J. Geophys. Res.,* **101,** 22 869–22 889.

Diaz, J. P., M. Arbelo, F. J. Exposito, G. Podesta, J. M. Prospero, and R. Evans, 2001: Relationship between errors in AVHRR-derived sea surface temperature and the TOMS Aerosol Index. *Geophys. Res. Lett.,* **28,** 1989–1992.

Dickerson, R. R., S. Kondragunta, G. Stenchikov, K. L. Civerolo, B. Doddridge, and B. N. Holben, 1997: The impact of aerosols on solar ultraviolet radiation and photochemical smog. *Science,* **278,** 827–830.

Dubovik, O., and M. King, 2000: A flexible inversion algorithm for retrieval of aerosol optical properties from Sun and sky radiance measurements. *J. Geophys. Res.,* **105,** 20 673–20 696.

Eck, T. F., B. N. Holben, J. S. Reid, O. Dubovik, A. Smirnov, N. T. O'Neill, I. Slutsker, and S. Kinne, 1999: Wavelength dependence of the optical depth of biomass burning, urban and desert dust aerosols. *J. Geophys. Res.,* **104,** 31 333–31 349.

Ginoux, P., M. Chin, I. Tegen, J. Prospero, B. Holben, D. Dubovik, and S. J. Lin, 2001: Sources and distributions of dust aerosols simulated with the GOCART model. *J. Geophys. Res.,* **106,** 20 255–20 273.

Gleason, J. F., N. C. Hsu, and O. Torres, 1998: Biomass burning smoke measured using backscattered ultraviolet radiation: SCAR-B and Brazilian smoke interannual variability. *J. Geophys. Res.,* **103,** 31 969–31 978.

Gordon, H. R., T. Du, and T. Zhang, 1997: Remote sensing of ocean color and aerosol properties: Resolving the issue of aerosol absorption. *Appl. Opt.,* **36,** 8670–8684.

Herman, J. R., and E. Celarier, 1997: Earth surface reflectivity climatology at 340 and 380 nm from TOMS data. *J. Geophys. Res.,* **102,** 28 003–28 011.

——, P. K. Bhartia, O. Torres, C. Hsu, C. Seftor, and E. Celarier, 1997: Global distribution of UV-absorbing aerosols from *Nimbus7*/TOMS data. *J. Geophys. Res.,* **102,** 16 911–16 922.

——, N. Krotkov, E. Celarier D. Larko, and G. Labow, 1999: Distribution of UV radiation at the Earth's surface from TOMS-measured UV-backscattered radiances. *J. Geophys. Res.,* **104,** 12 059–12 076.

——, E. Celarier, and D. Larko, 2001: UV 380 nm reflectivity of the Earth's surface, clouds and aerosols. *J. Geophys. Res.,* **106,** 5335–5351.

Holben, B. N., and Coauthors, 1998: AERONET—A federated instrument network and data archive for aerosol characterization. *Remote Sens. Environ.,* **66,** 1–16.

Hsu, N. C., J. R. Herman, J. F. Gleason, O. Torres, and C. J. Seftor, 1999: Satellite detection of smoke aerosols over a snow/ice surface by TOMS. *Geophys. Res. Lett.,* **26,** 1165–1168.

——, ——, and C. Weaver, 2000: Determination of radiative forcing of Saharan dust using combined TOMS and ERBE data. *J. Geophys. Res.,* **105,** 20 649–20 661.

King, M. D., Y. J. Kaufman, D. Tanré, and T. Nakajima, 1999: Remote sensing of tropospheric aerosols from space: Past, present, and future. *Bull. Amer. Meteor. Soc.,* **80,** 2229–2259.

Krotkov, N. A., P. K. Bhartia, J. R. Herman, V. Fioletov, and J. Kerr, 1998: Satellite estimation of spectral surface UV irradiance in the presence of tropospheric aerosols. 1: Cloud-free case. *J. Geophys. Res.,* **103,** 8779–8793.

Litjens, R. A. J., T. I. Quickenden, and C. G. Freeman, 1999: Visible and near-ultraviolet absorption spectrum of liquid water. *Appl. Opt.,* **38,** 1216–1223.

McPeters, R. D., and Coauthors, 1996: Nimbus-7 Total Ozone Mapping Spectrometer (TOMS) data products user's guide. NASA Ref. Publ. 1384.

Miller, R. L., and I. Tegen, 1998: Climate response to soil dust aerosols. *J. Climate,* **11,** 3247–3267.

Mishchenko, M. I., I. V. Geogdzhayev, B. Cairns, W. B. Rossow, and A. A. Lacis, 1999: Aerosol retrievals over the ocean by use of channels 1 and 2 AVHRR data: Sensitivity analysis and preliminary results. *Appl. Opt.,* **38,** 7325–7341.

Nakajima, T., and A. Higurashi, 1998: A use of two-channel radiances for an aerosol characterization from space. *Geophys. Res. Lett.,* **25,** 3815–3818.

Patterson, E. M., D. A. Gillette, and B. Stockton, 1977: Complex index of refraction between 300 and 700 nm for Saharan aerosols. *J. Geophys. Res.,* **82,** 3153–3160.

Prospero, J. M., P. Ginoux, O. Torres, and S. E. Nicholson, 2002: Environmental characterization of global sources of atmospheric soil dust derived from the *Nimbus-7* TOMS absorbing aerosol product. *Rev. Geophys.,* in press..

Sokolik, I., A. Andronova, and T. C. Johnson, 1993: Complex refractive index of atmospheric dust aerosols. *Atmos. Environ.,* **27A,** 2495–2502.

Stowe, L. L., A. M. Ignatov, and R. R. Singh, 1997: Development, validation, and potential enhancements to the second-generation operational aerosol product at the National Environmental Satellite, Data, and Information Service of the National Oceanic and Atmospheric Administration. *J. Geophys. Res.,* **102,** 16 923–16 934.

Torres, O., and P. K. Bhartia, 1999: Impact of tropospheric aerosol absorption on ozone retrieval from backscattered ultraviolet measurements. *J. Geophys. Res.,* **104,** 21 569–21 577.

——, ——, J. R. Herman, Z. Ahmad, and J. Gleason, 1998: Derivation of aerosol properties from satellite measurements of backscattered ultraviolet radiation: Theoretical basis. *J. Geophys. Res.,* **103,** 17 099–17 110.

——, J. R. Herman, P. K. Bhartia, and A. Sinyuk, 2001: Aerosol properties from EP-TOMS near UV observations. *Adv. Space Res.,* in press.

van de Hulst, H. C., 1957: *Light Scattering by Small Particles.* John Wiley, 470 pp.